Available online at www.sciencedirect.com

ScienceDirect

journal homepage: www.elsevier.com/locate/he

Evaluation of interfacial pH change during water splitting at pulsed regime using finite element method

Gabriel Wosiak [a], Mariana C. Silva [a], Jeyse da Silva [a], Evaldo B. Carneiro-Neto [a], Mauro C. Lopes [b], Ernesto Pereira [a,*]

[a] Chemistry Department, Federal University of São Carlos, 13565-905, São Carlos, SP, Brazil
[b] Departamento de Química, Universidade Estadual Do Centro-Oeste, 85040-080, Guarapuava, PR, Brazil

HIGHLIGHTS

- Depending on the operating condition, the interfacial pH changed up to 9 units.
- Finite element method can be used to investigate water splitting behavior.
- The use of pulsed current show superior energy efficiency.
- High temperature electrolysis attenuates the interfacial pH changes.

GRAPHICAL ABSTRACT

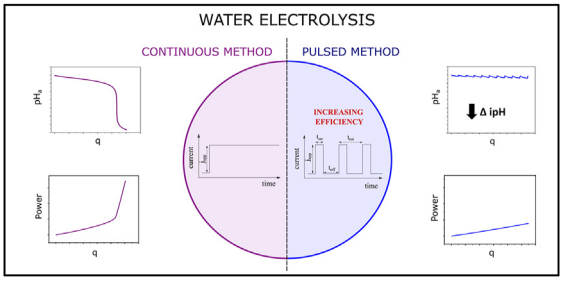

ARTICLE INFO

Article history:
Received 2 December 2020
Received in revised form
19 February 2021
Accepted 24 February 2021
Available online 5 April 2021

Keywords:
Interfacial pH
Finite element simulation
Water splitting

ABSTRACT

Electrochemical water splitting is a well-known reaction, investigated since 1869 due to its wide applicability for different purposes. Despite occurring at the electrode/solution interface, this set of reactions can be governed not only by interfacial properties but also by reactant transport from the solution toward the electrode surface. For water splitting specifically, the reaction mechanism itself leads to a pH change at the interface although the bulk value remains constant. In this work, we simulated such pH variations using the finite element method. The results show an interfacial pH change of up to 9 pH units. This modification in the reaction condition affects many related parameters such as electric power consumption, which increases. Thence, we investigated the effect of using an AC perturbation. In the conditions we have studied, it is observed an important delay in the pH change, although it always occurs.

* Corresponding author.
E-mail address: ernesto@ufscar.br (E. Pereira).
https://doi.org/10.1016/j.ijhydene.2021.02.195

Nomenclature

Abbreviations

ipH	Interfacial pH
FEM	Finite Element Method
HER	Hydrogen Evolution Reaction
OER	Oxygen Evolution Reaction

Symbols

α_i	Activity of specie *i*
η	Total overpotential (V)
η_{ac}	Activation overpotential (V)
η_a	Anodic overpotential (V)
η_{bub}	Bubble overpotential (V)
η_{conc}	Concentration overpotential (V)
η_c	Cathodic overpotential (V)
η_R	Resistance overpotential (V)
ω	Pulse frequency (*Hz*)
D_i	Diffusion coefficient of specie *i* ($cm^2\ s^{-1}$)
DC	Duty Cycle
E^0	Standard potential (V)
E_a^0	Anodic standard potential (V)
E_c^0	Cathodic standard potential (V)
E_a	Anodic cell potential (V)
E_{cell}	Cell potential (V)
E_c	Cathodic cell potential (V)
f_i	Fugacity of specie *i*
ipH_a	Interfacial pH at anode surface
ipH_c	Interfacial pH at cathode surface
j_{app}	Applied current density ($mA\ cm^{-2}$)
q	Charge (C)
T	Temperature (°C)
t	Time (s)
t_{off}	Pulse off time (s)
t_{on}	Pulse on time (s)
t_{tot}	Cycle time (s)

Physical constants

F	Faraday constant 96485.3329 C mol^{-1}
R	Ideal gas constant 8.3144621 J K^{-1} mol^{-1}

Introduction

The increasing energy demand, along with the environmental concern, has fueled the search for renewable and sustainable energy sources [1–5]. In this context, the use of hydrogen has been pointed out as a promising alternative to replace fossil fuels, due to its high energy density (120 MJ kg^{-1}) [6–8] as well as the fact of being more environmentally friendly. However, some issues must be overcome for this technology to become feasible. Currently, hydrogen production takes place mainly from natural gas in a process of efficiency between 50–75% [9,10] that also releases CO_2. In this scenario, water electrolysis stands out as the most sustainable H_2 production methodology, since does not generate toxic by-products, uses renewable energy sources, and leads to a high purity gas [11,12]. For industrial applications, concentrated *KOH* is the most used medium for water electrolysis, although this reaction can be performed in acidic or alkaline media [13–15].

The following chemical equations describe the anodic and cathodic charge transfer reactions for water electrolysis.

For acidic media:

$$2H^+_{(aq)} + 2e^- \rightleftharpoons H_{2(g)} \quad E^0 = 0.000V \tag{1}$$

$$H_2O_{(1)} \rightleftharpoons \frac{1}{2}O_{2(g)} + 2H^+_{(aq)} + 2e^- \quad E^0 = 1.229V \tag{2}$$

And, for alkaline media:

$$2H_2O_{(1)} + 2e^- \rightleftharpoons H_{2(g)} + 2OH^-_{(aq)} \quad E^0 = -0.828V \tag{3}$$

$$2OH^- \rightleftharpoons O_{2(g)} + H_2O_{(1)} + 2e^- \quad E^0 = 0.401V \tag{4}$$

Then, there is the production or the consumption of H^+ and/or OH^- species at the electrode/electrolyte interface, which causes a concentration gradient near the electrode surface resulting in an interfacial pH change [16,17]. Considering a non-polarizable interface, the cell potential E_{cell} in the HER [18,19], is the sum of the Nernst potential E^0, different overpotentials η for the anodic and cathodic reactions, as shown by Equation (5), as follows.

$$E_{cell} = E^0_{rxn} + \eta = E^0_c - E^0_a + \eta_c - \eta_a \tag{5}$$

Besides, according to Leistra et al. [20], η is, by itself, the sum of eight components: concentration overpotential η_{conc}, activation overpotential η_{ac}, resistance overpotential η_R, and bubble's formation overpotential η_{bub}. There are four terms for the cathodic reaction and four for the anodic one. Equation (6) is valid for any electrochemical process, and one important issue is that the overpotential components are not independent of each other. Each of these components is related to the water-splitting reaction and is influenced by an interfacial pH change [21,22].

$$\eta = \eta_{conc} + \eta_{ac} + \eta_R + \eta_{bub} \tag{6}$$

The concentration overpotential occurs due to the presence of a concentration gradient which is related to the consumption and production of H^+ and OH^- species at the electrode surface, then it is related to any interface pH change which could occur. The activation overpotential is the focus of recent research in the literature [23–25], and it is mainly related to the development of new electrode materials [26]. Also, it is important to point out that the catalytic activity of any material can also be strongly affected by the interfacial pH value and/or changes, as described by Hamann [27]. The resistance overpotential is the cause of an important part of energy consumption in electrolyzers. Then, both cell geometry and electrolyte conductivity have already been optimized to reduce their value. The bubble's overpotential influences all of the overpotentials described above for different reasons [28]. One aspect is that the gas evolution blocks part of the electrode surface, decreasing the active sites availability, and, then, it could be associated with the activation overpotential. The dissolved gas near the electrode surface could act during the bubble's growth, then, decreasing the amount of hydrogen formed at the electrode surface, modifying the concentration

overpotential. The presence of bubbles also affects the displacement of reagents in the solution, leading to the formation of a solvent flux, which could affect different components of the overpotential [29]. For HER reaction, the bubble characteristics also depend on the interfacial pH.

The variation in the interfacial pH can also change the mechanisms of water splitting, causing an increase in the E^0_{rxn}. For example, for a given acidic pH value, the cathodic reaction is predominantly the proton reduction [30]. But if a negative current density flowing through the interface is high enough, the consumption of protons leads to an increase in the interfacial pH at the cathode [31]. Thus, depending on the experimental conditions, water (and not proton) reduction becomes significant. This transition mechanism is followed by a change in the formal potential of the reaction. The same reasoning is valid for water oxidation in alkaline media. Taking into account these points, an efficient form to investigate all these possibilities together or even give special attention to some of them is the use of computational methods [32,33].

Computational simulations are a valuable tool to guide, evaluate, and even give quantitative information about the system's properties that cannot be easily accessed experimentally [34]. Multiphysics modeling by the Finite Element Method (FEM) is a well-established technique to describe many engineering problems. In the last years, electrochemical processes have also been studied using this approach [35–40], summarizing a lot of fundamental discussions without the need to obtain analytical solutions for the partial differential equations necessary to describe them. It allows the study of the mechanism(s) in a multitude of boundary conditions [41].

In previous work, we proposed a model for the calculation of interfacial pH changes during HER [42]. The proposed model considers the transport only by diffusion, which is reasonable in voltammetric and chronoamperometric experiments. But when it is necessary to model high current values, the transport via migration dominates, and it is necessary to simulate a tertiary current distribution, which includes parameters describing each ion, and for the supporting electrolyte, i.e., to use the Nernst-Planck equation and even consider the ohmic drop in the electrolyte. To validate the model we show in the Supplementary material comparison between the experimental interfacial pH variation reported by Zimer et Al [43], and the results obtained by a 2D axisymmetric simulation for the rotating ring-disk electrode.

It is also proposed in the literature that pulsed methods can change the characteristics of electrochemical processes, and it is commonly used in electrodeposition to control the deposit morphology [44–47]. In general, these are mass-transfer limited processes, then the use of pulsed methods with changeable parameters allows the restitution of the reactant to the diffusion layer. In the HER field, some works describe an improvement in efficiency by decreasing the cell potential using pulsed methods [48–52]. As well as in the electrodeposition, the choice of parameters is of main importance to improve this energy efficiency increase. As an example, ultrashort pulses can be strongly affected by the electrode double layer charging, spending energy with polarization instead of with a faradaic reaction [53].

Taking into account the need to develop new methods for obtaining sustainable energy, and aiming to increase the energy efficiency for this reaction, in this work we use a computational model to simulate pulsed electrolysis, and thereby demonstrate the increase in the energy efficiency of the hydrogen evolution reaction compared to conventional non-pulsed methods. In this sense, one of the main goals of this work is to investigate a large set of parameter values that influence interfacial pH during water electrolysis.

Theory and simulation procedure

As our focus is on the local pH variation, we have kept the model as simple as possible to capture the phenomenon of interest. Therefore, we considered a one-dimensional electrolyte bounded by two non-porous electrodes. The tertiary current distribution (Nernst-Planck Poisson equations) assuming a stationary solution and a binary electrolyte was calculated. The electrode reactions 1–4 were modeled by the Butler-Volmer equation and the recombination of electroactive species, H^+ and OH^-, was considered. The model implementation was similar to our previous work [42] modified as follows. Considering the high concentrations and current densities to be modeled, the migration of electroactive species under electric potential gradient was admitted. To carry out the simulations in the galvanostatic mode, the applied potential was calculated to match the sum of all the contributions of formal potentials and overpotentials for a given applied current density. This is done by solving a weak expression for each electrode in which the variable to be minimized is the applied potential corresponding to each operating condition, which is analogous to the electronic control used in potentiostats to perform a galvanostatic experiment [34].

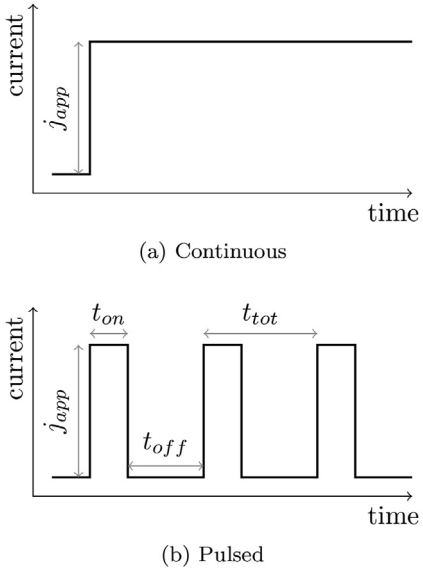

Fig. 1 – Profile of the general continuous (a) and pulsed (b) methods showing the investigated changeable parameters.

Fig. 1 is a generic representation of the studied current profiles in continuous and pulsed experiments. In the first case it is possible to control only the current density, and in the second case two additional parameters, defined by Equations (7)–(9), can be varied. The frequency ω and the duty cycle, *DC*, determine the pulse time (t_{on}) and the open-circuit time (t_{off}).

$$t_{tot} = t_{on} + t_{off} \tag{7}$$

$$\omega = \frac{1}{t_{tot}} \tag{8}$$

$$DC = \frac{t_{on}}{t_{tot}} \tag{9}$$

To simulate the increase in the mass transport with the temperature, we modify the diffusion coefficients of OH^- and H^+ to the values reported by Lee et Al [54]. at 20 and 50°C. Table 1 shows the chosen parameters which were investigated using a factorial design procedure. For comparison, the continuous experiments were also carried out in both temperatures, keeping the total charge constant.

The set of differential equations for a tertiary current distribution was solved by a time-dependent solver from the software COMSOL Multiphysics 5.2 with the Electrochemistry module, in a computer operating with Ubuntu 18.04.2 LTS with 1 physical processor Intel(R) Core(TM) i7-8700 and 32 Gb of RAM. The computational time to perform the simulations is dependent on the number of pulses, where shorter time steps are necessary to evaluate the pH along with the domain. While the continuous experiments took only a few minutes to perform the calculations, the longest experiment studied in this work (Fig. 6, pulsed) lasted 14 h.

Results and discussion

Continuous experiment

Fig. 2 shows the interfacial pH at the anode and cathode in acid (pH = 3) and alkaline media (pH = 11) during 1 s of the electrolysis and the consequent cell potential required to keep the current density constant. It is worth noting the sharp increase in the interfacial pH at the cathode for acid media, and at the anode for alkaline media, while only a moderate pH variation at the cathode (alkaline) and the anode (acidic) occurs. As a consequence, the sharp increase in the cell potential

Table 1 – Chosen pulse parameters (ω = frequency; DC = Duty Cicle; t_{on}; t_{off}) and electrolyte temperature (T).

Exp.	ω (Hz)	DC	T (°C)	t_{on} (s)	t_{off} (s)
1	1	0.1	20	0.1	0.9
2	1	0.1	50	0.1	0.9
3	1	0.5	20	0.5	0.5
4	1	0.5	50	0.5	0.5
5	10	0.1	20	0.01	0.09
6	10	0.1	50	0.01	0.09
7	10	0.5	20	0.05	0.05
8	10	0.5	50	0.05	0.05

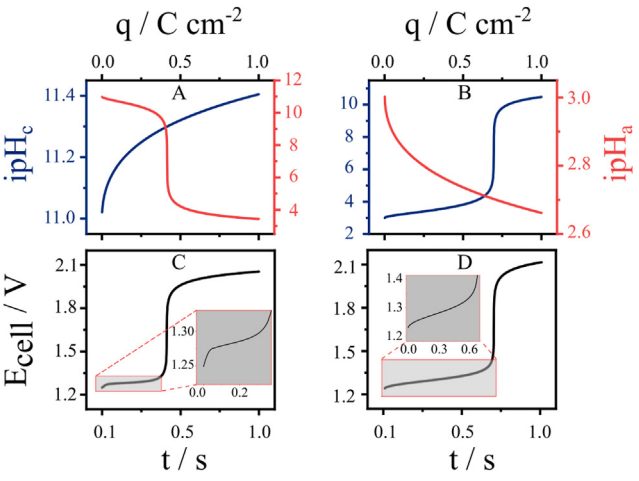

Fig. 2 – Comparison between interfacial pH at the anode (red) and cathode (blue) surfaces and the cell potential (black) during the water electrolysis at 1 mA cm^{-2} in (A,B) alkaline (pH = 11) and (C,D) acid (pH = 3) media. (For interpretation of the references to color in this figure legend, the reader is referred to the Web version of this article.)

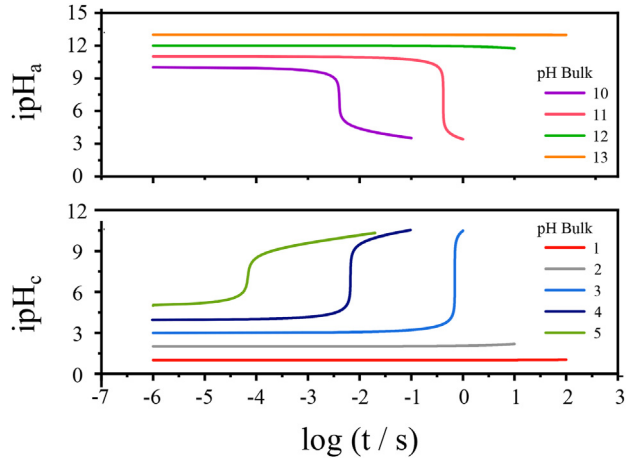

Fig. 3 – Comparison between interfacial pH at (A) anode for alkaline experiments and at (B) cathode surface for acid media at different values of bulk pH. (pH = 1, 2, 3 and 5 to figure A; pH = 10, 11, 12 and 13 to figure B), during the water electrolysis at 1 mA cm^{-2}.

is driven by the concentration overpotential respectively at the cathode for alkaline electrolysis and the anode for acidic electrolysis. Due to the difference in the diffusion coefficient between H^+ and OH^-, the transition time is shorter in alkaline media. In both cases, there is a dramatic change of almost 9 pH units. This means, that the pH value at the interface is completely different from the bulk value. The first important consequence is an increase in the electrical energy consumption since the cell potential increases, whose experimental evidence was reported by Baniasadi et al. [16]. Second, this pH change could turn the electrode materials chemically unstable since they were designed for a different experimental condition [22,55,56].

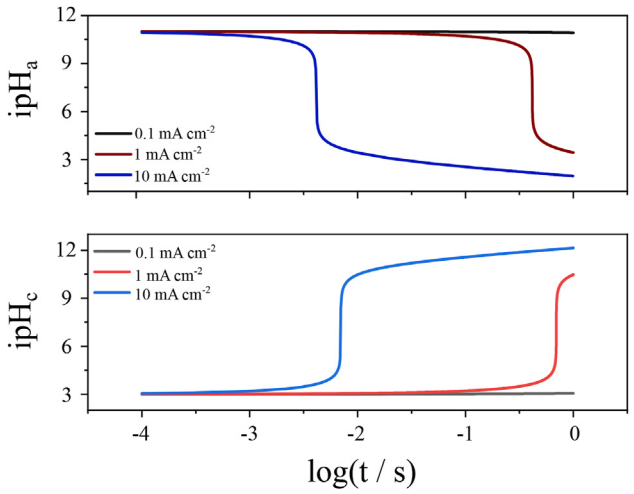

Fig. 4 – Influence of the current density on the interfacial pH for bulk pH levels pH 3 (A) and 11 (B).

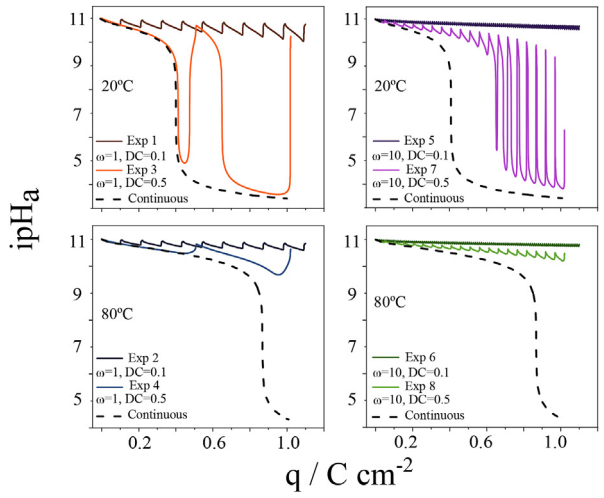

Fig. 5 – Interfacial pH profile as a function of charge for the 8 pulsed experiments in comparison to the continuous electrolysis in the same conditions for each case (varying: frequency, Duty Cycle, and temperature) (j = 1 mA cm^{-2}).

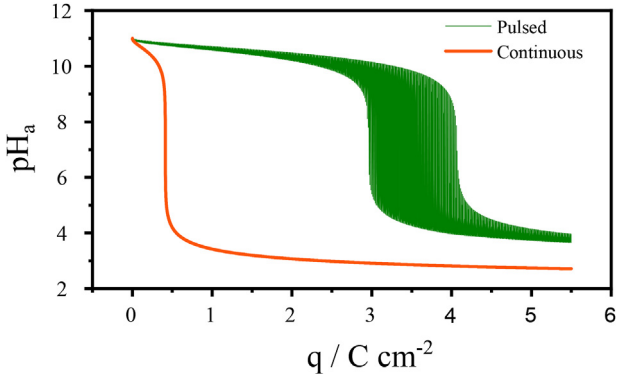

Fig. 6 – Interfacial pH at the anode surface during water electrolysis for continous and pulsed experiment (j = 1 mA cm^{-2}, ω = 10 Hz, DC = 0.1).

Fig. 3 shows the influence of bulk pH on the interfacial pH profile. Before the transition, the pH varies slowly due to the self-buffering action of the recombination reaction. Therefore, the closer the bulk pH is to the neutral value, the faster the transition, owing to the lower excess of H^+ or OH^-. When the bulk pH reaches extreme values, a large period of time and/or larger currents are necessary to observe an interfacial pH transition, but it still occurs. It implies that every non-buffered electrolysis that involves H^+ or OH^- species has a fast change in interfacial pH. It is also important to note that the self-buffering action of the recombination reaction is also present after the transition and at the electrode that does not undergo the transition, causing moderate but significant variation of pH. Since the self-buffering action decreases as the bulk pH approaches the neutral value, the changes become progressively more uniform in both electrodes (see Fig. S1 in the supplementary information). It is important to stress out that in all the cases presented in Fig. 3, an important change in the cell potential is also observed, i.e., the energy cost increased.

Fig. 4 shows that an increase in the current density can drive a faster interfacial pH variation, as expected. For example, using 10 mA cm^{-2} causes the changes to reach 9 pH units at approximately 10 ms. This abrupt change occurs due to the concentration of H^+ ions being only 10^{-3} mol L^{-1} and, to maintain the reaction rate corresponding to 10 mA cm^{-2}, there is a rapid consumption of these ions at the interface, causing their concentration to reach 10^{-9} mol L^{-1}, occasion in which the diffusion and migration transport mechanism and the water autoionization process start to supply the demand for species at the interface generated by the imposed reaction rate.

Considering what was exposed in the text above, we will now discuss the application of pulsed current during water electrolysis.

Pulsed method

Fig. 5 shows some representative pH and potential profiles comparing pulsed and continuous electrolysis at different temperatures, DC and ω. The recovering of the OH^- interfacial concentration during the open circuit period can be clearly distinguished in the pulsed electrolysis. Comparing different DC, there is no pH transition for DC = 0.1 until the charge of 1 °C cm^{-2}, and the transition occurs for DC = 0.5, in both frequencies. This effect could be related to the total relaxation time, which becomes larger as the DC decreases. The consequence of an increase in the frequency and a decrease in the DC is a smaller variation in the interfacial pH, and then, in the cell potential. Some electrolyzers work at high temperatures, and, in this case, the heat is another energy source to support the water electrolysis. Then, we decide to simulate the temperature effect on the interfacial pH modifying the diffusion coefficients of H^+ and OH^- species. At high temperatures, the process is favored by reducing the ohmic drop in the solution [57], since lowering the solution viscosity makes the transport of species in the solution faster, and, finally, the activation barrier to perform the process is slightly reduced. A rise in the temperature always delays the transition time, as a result of the increase in transport (diffusion coefficients). This is a way

to understand the greater efficiency of high-temperature electrolysis. It also decreases the pH variation in all pulsed experiments, delaying the transition.

We represented separately experiment number 5 for a greater charge interval in Fig. 6 to show that the transition occurs at a high charge. Comparing with continuous electrolysis, a charge 3 times higher has evolved before the pH transition which immediately implies less energy consumption.

In a real electrolyzer some factors, such as electrolyte circulation can decrease the pH variation, while others, such as electrode porosity, can increase the effect. However, some reported potential profiles show the abrupt transition in the cell potential as predicted in the present work (see Figure 9 of Vincent et al. [48], for example), showing that, despite the simplicity of our approach, it captures an essential feature of the system. Furthermore, it is conceptually very important because it shows that avoiding such a transition is a fundamental technological challenge.

Fig. 7A shows the electrical energy spent (dissipated) during the water electrolysis reaction. When the interfacial pH (Fig. 5) has a transition, a significant raise in the needed power to perform the electrolysis is observed. The pulsed method can retard the transition, decreasing the energy spent to produce the same product quantity. In experiments 1, 2, 5, and 6 (DC = 0.1), where the pH transition is not observed, the dissipated power is much lower when using lower duty cycle values. Experiments 3 and 7 (DC = 0.5, 20 °C) present a higher dissipated power than experiments 4 and 8 (DC = 0.5, 50 °C). In this case, an increase in the temperature avoided the pH transition, and consequently, the dissipated power was lower probably related to the increase in the mass transport in the solution. Fig. 7B shows a bar representation of the dissipated power for electrolysis of 1 °C cm^{-2} for Experiment 6 compared to the continuous current perturbation at the same temperature. This result shows the importance of interfacial pH control in the energy spent. The continuous experiment presents an interfacial pH transition, and as a consequence, spends more energy during the electrolysis. Under the same charge, there is no pH transition, and, therefore, the dissipated power is a linear function of the charge. These data are summarized in Fig. 7B. Here, the dissipated power for all experiments is presented. As can be observed, pulsed experiments have up to 10% of the continuous ones. Finally, Fig. 7C presents the Pareto plots about the effect of the control variables (frequency, duty cycle, and temperature) over the dissipated power during the reaction. As can be easily observed, the most important parameters are the duty cycle (parameter B) and the temperature (parameter C). The duty cycle increase leads to an increase in the dissipated power. This is an expected result because as DC increases, the pH transition occurs in a shorter time. On the contrary, the temperature decreases the power consumption which is also an expected result because as the temperature increases, the solution viscosity decreases leading to an increase in the rate of mass transport in the solution. A third effect is important which is the cross effect between the temperature and the duty cycle. It is important to stress out that this is not a direct effect in the dissipated power itself, instead, it means how the expected value is different from the simulated one. That is, if there is not a significant cross effect, its value is near zero, as is observed for the value of the cross effects A*C, A*B, and A*B*C. In this case, the explanation for the observed result is that the increase in the temperature is more important than an increase in the duty cycle.

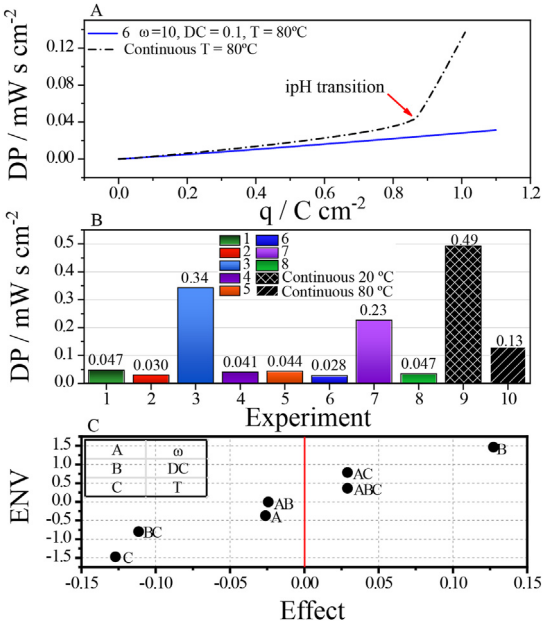

Fig. 7 – (A) Dissipated power as a function of charge for each pulsed experiment (1–8) in comparison with the continuous electrolysis (to 20 and 50 °C); (j = 1 mA cm^{-2}, q = 1 °C cm^{-2}), (B) Bar graph of pulsed experiments (1–8) in comparison to continuous (9–10), (C) Probability graph of significant effects of the variables on pulsed experiments. DP = Dissipated Power ENV = Expected normal value.

Conclusions

The present work demonstrates that interfacial pH control has a strong importance in the energetic consumption to produce hydrogen gas. An explanation about the higher efficiency of pulsed and high-temperature electrolysis in terms of interfacial pH is presented. Even for low current densities, there are significant pH variations in both electrodes when the bulk pH is near neutral. In intermediate bulk pH, the use of pulsed current can postpone the pH transition and, when it occurs, the cell potential is lower than in continuous experiments. The increase in frequency ω reduces the pH changes without changing the experiment time, and reducing the duty cycle, the electrolysis has more time to relax, and it reduces considerably the concentration overpotential.

Declaration of competing interest

The authors declare that they have no known competing financial interests or personal relationships that could have appeared to influence the work reported in this paper.

Acknowledgments

The support of this research by FAPESP (grants: 2013/07296-2, 2014/50249-8, 2015/12851-0, 2017/11986-5, 2018/24383-0), Shell, CNPq, and CAPES (Code 001).

Appendix A. Supplementary data

Supplementary data to this article can be found online at https://doi.org/10.1016/j.ijhydene.2021.02.195.

REFERENCES

[1] Chu S, Majumdar A. Opportunities and challenges for a sustainable energy future. Nature 2012;488(7411):294–303. https://doi.org/10.1038/nature11475.

[2] Chang CY. A critical analysis of recent advances in the techniques for the evaluation of renewable energy projects. Int J Proj Manag 2013;31(7):1057–67. https://doi.org/10.1016/j.ijproman.2013.03.001. URL, https://linkinghub.elsevier.com/retrieve/pii/S0263786313000379.

[3] Ganiyu SO, Martínez-Huitle CA, Rodrigo MA. Renewable energies driven electrochemical wastewater/soil decontamination technologies: a critical review of fundamental concepts and applications. Appl Catal B Environ 2020;270:118857. https://doi.org/10.1016/j.apcatb.2020.118857. URL, https://linkinghub.elsevier.com/retrieve/pii/S0926337320302721.

[4] Kothari R, Tyagi V, Pathak A. Waste-to-energy: a way from renewable energy sources to sustainable development. Renew Sustain Energy Rev 2010;14(9):3164–70. https://doi.org/10.1016/j.rser.2010.05.005. URL, https://linkinghub.elsevier.com/retrieve/pii/S1364032110001437.

[5] Pareek A, Dom R, Gupta J, Chandran J, Adepu V, Borse PH. Insights into renewable hydrogen energy: recent advances and prospects. Mater Sci Energy Technol 2020;3:319–27. https://doi.org/10.1016/j.mset.2019.12.002. URL, https://linkinghub.elsevier.com/retrieve/pii/S258929912030001X.

[6] Verbruggen A, Fischedick M, Moomaw W, Weir T, Nadaï A, Nilsson LJ, et al. Renewable energy costs, potentials, barriers: conceptual issues. Energy Pol 2010;38(2):850–61. https://doi.org/10.1016/j.enpol.2009.10.036.

[7] Petrov O, Bi X, Lau A. Impact assessment of biomass-based district heating systems in densely populated communities. Part II: would the replacement of fossil fuels improve ambient air quality and human health? Atmos Environ 2017;161:191–9. https://doi.org/10.1016/j.atmosenv.2017.05.001. URL.

[8] Bamati N, Raoofi A. Development level and the impact of technological factor on renewable energy production. Renew Energy 2020;151:946–55. https://doi.org/10.1016/j.renene.2019.11.098.

[9] Baykara SZ. Hydrogen: a brief overview on its sources, production and environmental impact. Int J Hydrogen Energy 2018;43(23):10605–14. https://doi.org/10.1016/j.ijhydene.2018.02.022. URL, https://linkinghub.elsevier.com/retrieve/pii/S0360319918304002.

[10] Wang M, Wang G, Sun Z, Zhang Y, Xu D. Review of renewable energy-based hydrogen production processes for sustainable energy innovation. Global Energy Interconnect 2019;2(5):436–43. https://doi.org/10.1016/j.gloei.2019.11.019. URL, https://linkinghub.elsevier.com/retrieve/pii/S2096511719301100.

[11] Ayodele BV, Abdullah TARBT, Alsaffar MA, Mustapa SI, Salleh SF. Recent advances in renewable hydrogen production by thermo-catalytic conversion of biomass-derived glycerol: overview of prospects and challenges. Int J Hydrogen Energy 2020;45(36):18160–85. https://doi.org/10.1016/j.ijhydene.2019.08.002. URL, https://linkinghub.elsevier.com/retrieve/pii/S0360319919329118.

[12] Momirlan M, Veziroglu T. The properties of hydrogen as fuel tomorrow in sustainable energy system for a cleaner planet. Int J Hydrogen Energy 2005;30(7):795–802. https://doi.org/10.1016/j.ijhydene.2004.10.011. URL, https://linkinghub.elsevier.com/retrieve/pii/S0360319904003398.

[13] Schalenbach M, Tjarks G, Carmo M, Lueke W, Mueller M, Stolten D. Acidic or alkaline? Towards a new perspective on the efficiency of water electrolysis. J Electrochem Soc 2016;163(11):F3197–208. https://doi.org/10.1149/2.0271611jes. URL, https://iopscience.iop.org/article/10.1149/2.0271611jes.

[14] Dawood F, Anda M, Shafiullah GM. Hydrogen production for energy: an overview. Int J Hydrogen Energy 2020;45(7):3847–69. https://doi.org/10.1016/j.ijhydene.2019.12.059. URL.

[15] König A, Marquardt W, Mitsos A, Viell J, Dahmen M. Integrated design of renewable fuels and their production processes: recent advances and challenges. Curr Opin Chem Eng 2020;27:45–50. https://doi.org/10.1016/j.coche.2019.11.001. URL, https://linkinghub.elsevier.com/retrieve/pii/S221133981930053X.

[16] Baniasadi E, Dincer I, Naterer G. Electrochemical analysis of seawater electrolysis with molybdenum-oxo catalysts. Int J Hydrogen Energy 2013;38(6):2589–95. https://doi.org/10.1016/j.ijhydene.2012.11.106. URL, https://linkinghub.elsevier.com/retrieve/pii/S0360319912025955.

[17] Hoshino K, Furuya S, Buchheit RG. Effect of solution pH on layered double hydroxide formation on electrogalvanized steel sheets. J Mater Eng Perform 2019;28(4):2237–44. https://doi.org/10.1007/s11665-019-03963-x.

[18] Heusler KE, Gileadi E. In: Electrode kinetics for chemists, chemical engineers and material scientists. Weinheim, New York, Basel, Cambridge, Tokyo: VCH; 1993, ISBN 3-527-89561-2. https://doi.org/10.1002/bbpc.19940980425. 597 S., Preis: DM 189,-. Berichte der Bunsengesellschaft für physikalische Chemie 1994;98(4):644–645. URL.

[19] Shimizu N, Hotta S, Sekiya T, Oda O. A novel method of hydrogen generation by water electrolysis using an ultra-short-pulse power supply. J Appl Electrochem 2006;36(4):419–23. https://doi.org/10.1007/s10800-005-9090-y. URL.

[20] Leistra JA, Sides PJ. Voltage components at gas evolving electrodes. J Electrochem Soc 1987;134(10):2442–6. https://doi.org/10.1149/1.2100218. URL.

[21] Tsai WL, Hsu PC, Hwu Y, Chen CH, Chang LW, Je JH, et al. Building on bubbles in metal electrodeposition. Nature 2002;417(6885):139. https://doi.org/10.1038/417139a. URL.

[22] Hashemi H, S M, Modestino MA, Psaltis D. A membrane-less electrolyzer for hydrogen production across the pH scale. Energy Environ Sci 2015;8(7):2003–9. https://doi.org/10.1039/c5ee00083a.

[23] Juodkazytė J, Seniutinas G, Šebeka B, Savickaja I, Malinauskas T, Badokas K, et al. Solar water splitting: efficiency discussion. Int J Hydrogen Energy 2016;41(28):11941–8. https://doi.org/10.1016/j.ijhydene.2016.05.079. URL, https://linkinghub.elsevier.com/retrieve/pii/S0360319916300039.

[24] El-Askary WA, Sakr IM, Ibrahim KA, Balabel A. Hydrodynamics characteristics of hydrogen evolution process through electrolysis: numerical and experimental studies. Energy 2015;90:722–37. https://doi.org/10.1016/j.energy.2015.07.108. URL.

[25] Andrews J, Shabani B. Re-envisioning the role of hydrogen in a sustainable energy economy. Int J Hydrogen Energy 2012;37(2):1184–203. https://doi.org/10.1016/j.ijhydene.2011.09.137. URL, https://linkinghub.elsevier.com/retrieve/pii/S0360319911022841.
[26] Kovendhan M, Kang H, Youn JS, Cho H, Jeon KJ. Alternative cost-effective electrodes for hydrogen production in saline water condition. Int J Hydrogen Energy 2019;44(11):5090–8. https://doi.org/10.1016/j.ijhydene.2018.08.038. URL, https://linkinghub.elsevier.com/retrieve/pii/S0360319918325473.
[27] Hamann CH, Hamnett A, Vielstich W. Electrochemistry. 2. auflage ed. Weinheim: Wiley-VCH Verlag GmbH & Co. KGaA; 2007, ISBN 9783527310692.
[28] Ernst S, Hamann CH. The pH-dependence of the hydrogen exchange current density at smooth platinum in alkaline solution (KOH). J Electroanal Chem 1975;60(1):97–100. https://doi.org/10.1016/S0022-0728(75)80206-3. URL, https://linkinghub.elsevier.com/retrieve/pii/S0022072875802063.
[29] Angulo A, van der Linde P, Gardeniers H, Modestino M, Fernández Rivas D. Influence of bubbles on the energy conversion efficiency of electrochemical reactors. Joule 2020;4(3):555–79. https://doi.org/10.1016/j.joule.2020.01.005. URL, https://linkinghub.elsevier.com/retrieve/pii/S2542435120300325.
[30] Santos J, Trivinho-Strixino F, Pereira E. Investigation of Co(OH)2 formation during cobalt electrodeposition using a chemometric procedure. Surf Coating Technol 2010;205(7):2585–9. https://doi.org/10.1016/j.surfcoat.2010.10.005. URL, https://linkinghub.elsevier.com/retrieve/pii/S0257897210010042.
[31] Abbasi T, Abbasi S. Renewable' hydrogen: prospects and challenges. Renew Sustain Energy Rev 2011;15(6):3034–40. https://doi.org/10.1016/j.rser.2011.02.026. URL, https://linkinghub.elsevier.com/retrieve/pii/S1364032111000748.
[32] Critelli RA, Bertotti M, Torresi RM. Probe effects on concentration profiles in the diffusion layer: computational modeling and near-surface pH measurements using microelectrodes. Electrochim Acta 2018;292:511–21. https://doi.org/10.1016/j.electacta.2018.09.157. URL, https://linkinghub.elsevier.com/retrieve/pii/S0013468618321534.
[33] Vyroubal P, Kazda T, Mačák M. Finite methods for lithium ion battery simulation. ECS Trans 2018;87(1):389–95. https://doi.org/10.1149/08701.0389ecst. URL, https://iopscience.iop.org/article/10.1149/08701.0389ecst.
[34] Nann T, Heinze J. Simulation in electrochemistry using the finite element method part 2: scanning electrochemical microscopy. Electrochim Acta 2003;48(27):3975–80. https://doi.org/10.1016/S0013-4686(03)00312-8.
[35] Aldas K, Pehlivanoglu N, Mat M. Numerical and experimental investigation of two-phase flow in an electrochemical cell. Int J Hydrogen Energy 2008;33(14):3668–75. https://doi.org/10.1016/j.ijhydene.2008.04.047. URL, https://linkinghub.elsevier.com/retrieve/pii/S0360319908004734.
[36] Anjos GR, Mangiavacchi N, Pontes J. Three-dimensional finite element method for rotating disk flows. J Braz Soc Mech Sci Eng 2014;36(4):709–24. https://doi.org/10.1007/s40430-013-0120-0. URL, http://link.springer.com/10.1007/s40430-013-0120-0.
[37] Abdin Z, Webb C, Gray E. Modelling and simulation of an alkaline electrolyser cell. Energy 2017;138:316–31. https://doi.org/10.1016/j.energy.2017.07.053. URL, https://linkinghub.elsevier.com/retrieve/pii/S0360544217312288.
[38] Arulrajan AC, Renault C, Lai SCS. How changes in interfacial pH lead to new voltammetric features: the case of the electrochemical oxidation of hydrazine. Phys Chem Chem Phys 2018;20(17):11787–93. https://doi.org/10.1039/C8CP01835A. URL, http://xlink.rsc.org/?DOI=C8CP01835A.
[39] Osafi M, Bakhshi Ani A, Kalbasi M. Numerical modeling of solid acid fuel cell performance with CsH2PO4- AAM (anodic alumina membrane) composite electrolyte. Int J Heat Mass Tran 2019;129:1086–94. https://doi.org/10.1016/j.ijheatmasstransfer.2018.10.049. URL, https://linkinghub.elsevier.com/retrieve/pii/S0017931018319902.
[40] Bott-Neto JL, Rodrigues MVF, Silva MC, Carneiro-Neto EB, Wosiak G, Mauricio JC, et al. Versatile spectroelectrochemical cell for in situ experiments: development, applications, and electrochemical behavior**. ChemElectroChem 2020;7(21):4306–13. https://doi.org/10.1002/celc.202000910. URL, https://onlinelibrary.wiley.com/doi/10.1002/celc.202000910.
[41] Dickinson EJ, Ekström H, Fontes E. COMSOL Multiphysics®: finite element software for electrochemical analysis. A mini-review. Electrochem Commun 2014;40:71–4. https://doi.org/10.1016/j.elecom.2013.12.020. URL, https://linkinghub.elsevier.com/retrieve/pii/S1388248113004840.
[42] Carneiro-Neto EB, Lopes MC, Pereira EC. Simulation of interfacial pH changes during hydrogen evolution reaction. J Electroanal Chem 2016;765:92–9. https://doi.org/10.1016/j.jelechem.2015.09.029. URL, https://linkinghub.elsevier.com/retrieve/pii/S1572665715301259.
[43] Zimer AM, Medina da Silva M, Machado EG, Varela H, Mascaro LH, Pereira EC. Development of a versatile rotating ring-disc electrode for in situ pH measurements. Anal Chim Acta 2015;897:17–23. https://doi.org/10.1016/j.aca.2015.09.047. URL, https://linkinghub.elsevier.com/retrieve/pii/S0003267015012052.
[44] Seyedraoufi Z, Mirdamadi S. Effects of pulse electrodeposition parameters and alkali treatment on the properties of nano hydroxyapatite coating on porous Mg–Zn scaffold for bone tissue engineering application. Mater Chem Phys 2014;148(3):519–27. https://doi.org/10.1016/j.matchemphys.2014.06.067. URL, https://linkinghub.elsevier.com/retrieve/pii/S0254058414004180.
[45] Balasubramanian A, Srikumar DS, Raja G, Saravanan G, Mohan S. Effect of pulse parameter on pulsed electrodeposition of copper on stainless steel. Surf Eng 2009;25(5):389–92. https://doi.org/10.1179/026708408X344680. URL, http://www.tandfonline.com/doi/full/10.1179/026708408X344680.
[46] Larson C, Farr JP. Current research and potential applications for pulsed current electrodeposition - a review. 2012. https://doi.org/10.1179/174591912X13238641755178.
[47] Larson C, Farr JPG. Recent advances in pulsed current electrodeposition: a brief review. Trans IMF 2010;88(5):237–42. https://doi.org/10.1179/174591910X12819621697975. URL, http://www.tandfonline.com/doi/full/10.1179/174591910X12819621697975.
[48] Vincent I, Choi B, Nakoji M, Ishizuka M, Tsutsumi K, Tsutsumi A. Pulsed current water splitting electrochemical cycle for hydrogen production. Int J Hydrogen Energy 2018;43(22):10240–8. https://doi.org/10.1016/j.ijhydene.2018.04.087. URL, https://linkinghub.elsevier.com/retrieve/pii/S0360319918312126.
[49] Dharmaraj CH, Adishkumar S. Economical hydrogen production by electrolysis using nano pulsed DC. Int J Energy Environ 2012;3(1):129–36.
[50] Huang C. Solar hydrogen production via pulse electrolysis of aqueous ammonium sulfite solution. Sol Energy 2013;91:394–401. https://doi.org/10.1016/j.solener.2012.09.009. URL, https://linkinghub.elsevier.com/retrieve/pii/S0038092X12003337.
[51] Saleet H, Abdallah S, Yousef E. The effect of electrical variables on hydrogen and oxygen production using a water electrolyzing system. Int J Appl Eng Res 2017;12(13):3730–9.

[52] Lin MY, Hourng LW. Effects of magnetic field and pulse potential on hydrogen production via water electrolysis. Int J Energy Res 2014;38(1):106–16. https://doi.org/10.1002/er.3112. URL.
[53] Shaaban AH. Water electrolysis and pulsed direct current. J Electrochem Soc 1993;140(10):2863–7. https://doi.org/10.1149/1.2220923. URL, https://iopscience.iop.org/article/10.1149/1.2220923.
[54] Lee SH, Rasaiah JC. Proton transfer and the mobilities of the H + and OH - ions from studies of a dissociating model for water. J Chem Phys 2011;135(12):124505. https://doi.org/10.1063/1.3632990. URL, http://aip.scitation.org/doi/10.1063/1.3632990.
[55] Yao Y, Gao X, Meng X. Recent advances on electrocatalytic and photocatalytic seawater splitting for hydrogen evolution. Int J Hydrogen Energy 2021;46(13):9087–100. https://doi.org/10.1016/j.ijhydene.2020.12.212. URL, https://linkinghub.elsevier.com/retrieve/pii/S0360319920348758.
[56] Fu J, Detsi E, De Hosson JT. Recent advances in nanoporous materials for renewable energy resources conversion into fuels. Surf Coating Technol 2018;347(2017):320–36. https://doi.org/10.1016/j.surfcoat.2018.05.001. URL, https://linkinghub.elsevier.com/retrieve/pii/S0257897218304687.
[57] Kuleshov N, Kuleshov V, Dovbysh S, Grigoriev S, Kurochkin S, Millet P. Development and performances of a 0.5 kW high-pressure alkaline water electrolyser. Int J Hydrogen Energy 2019;44(56):29441–9. https://doi.org/10.1016/j.ijhydene.2019.05.044. URL, https://linkinghub.elsevier.com/retrieve/pii/S0360319919318750.